THE JOURNAL OF BIOLOGICAL CHEMISTRY
Vol. 278, No. 50, Issue of December 12, pp. 50412–50421, 2003

Printed in U.S.A.

Dissecting Cooperative and Additive Binding Energetics in the Affinity Maturation Pathway of a Protein-Protein Interface*

Received for publication, June 26, 2003, and in revised form, September 23, 2003
Published, JBC Papers in Press, September 27, 2003, DOI 10.1074/jbc.M306848200

Jianying Yang‡§, Chittoor P. Swaminathan‡, Yuping Huang‡, Rongjin Guan‡, Sangwoo Cho‡, Michele C. Kieke¶‖, David M. Kranz¶, Roy A. Mariuzza‡, and Eric J. Sundberg‡**

From the ‡Center for Advanced Research in Biotechnology, W. M. Keck Laboratory for Structural Biology, University of Maryland Biotechnology Institute, Rockville, Maryland 20850 and the ¶Department of Biochemistry, University of Illinois, Urbana, Illinois 61801

When two proteins associate they form a molecular interface that is a structural and energetic mosaic. Within such interfaces, individual amino acid residues contribute distinct binding energies to the complex. In combination, these energies are not necessarily additive, and significant positive or negative cooperative effects often exist. The basis of reliable algorithms to predict the specificities and energies of protein-protein interactions depends critically on a quantitative understanding of this cooperativity. We have used a model protein-protein system defined by an affinity maturation pathway, comprising variants of a T cell receptor Vβ domain that exhibit an overall affinity range of ~1500-fold for binding to the superantigen staphylococcal enterotoxin C3, in order to dissect the cooperative and additive energetic contributions of residues within an interface. This molecular interaction has been well characterized previously both structurally, by x-ray crystallographic analysis, and energetically, by scanning alanine mutagenesis. Through analysis of group and individual maturation and reversion mutations using surface plasmon resonance spectroscopy, we have identified energetically important interfacial residues, determined their cooperative and additive energetic properties, and elucidated the kinetic and thermodynamic bases for molecular evolution in this system. The summation of the binding free energy changes associated with the individual mutations that define this affinity maturation pathway is greater than that of the fully matured variant, even though the affinity gap between the end point variants is relatively large. Two mutations in particular, both located in the complementarity determining region 2 loop of the Vβ domain, exhibit negative cooperativity.

Specific associations between heterologous proteins are required for many essential cellular processes. The biophysical factors that govern these protein-protein interactions, including van der Waals interactions, hydrogen bonding, hydrophobic packing, shape and charge complementarity, allostery, plasticity, and cooperativity (1–9), have been the subject of intensive study for decades. However, the formulation of reliable algorithms to predict the specificities and energies of these molecular interactions from protein structures alone has not been realized. Structural and energetic analyses of model protein-protein interactions have yielded some quantitative correlations on which to base such algorithms (1, 5, 10–15), but they remain far from comprehensive as some biophysical factors have resisted quantification or generalization.

Many studies have sought to establish such correlations based on the analysis of single-site residue mutations, which arose either naturally or by site-directed mutagenesis. Although this strategy can provide correlations for some factors that govern interactions, it is not possible to probe many of the more complex biophysical factors such as plasticity and cooperativity in this manner. Nonetheless, the interfaces of numerous protein complexes have been mapped energetically, primarily via alanine scanning mutagenesis, revealing that there often exists a significantly smaller functional epitope in which the majority of binding free energy resides (7). A complicating factor of single-site approaches is the common presence of nonadditivity of the individual binding energies of mutations within an interface, relative to the overall binding energy. Although there are instances of multiple mutations that are fully additive (16, 17), the summation of the changes in binding free energies of individual mutations is often less than (18–21) or greater than (18, 22–24) the wild type interaction. These latter two situations indicate that the binding energy is either less or more concentrated, respectively, within the hot spot residues tested relative to their individual analysis and that other non-hot spot residues may play important energetic roles in complex formation. Indeed, multiple mutations made concurrently to residues within an interface that do not interact directly can produce significant changes in binding free energy (23, 25, 26), indicative of the high degree of cooperative energetic effects on protein-protein interactions generally.

As nonadditivity of individual residue binding energies appears now to be common for molecular interactions, the dissection of such cooperative effects within protein interfaces is becoming increasingly important for a quantitative understanding of protein-protein interactions. A small, but growing, body of work has addressed this issue directly. Mutational analyses of human RNase inhibitor in complex with three different high affinity ligands have detected cooperative effects between both hot spot and non-hot spot residues based on enzyme kinetic and stopped-flow cytometric assays (22, 24, 27). Cooperativity has also been analyzed for residues that are

* This work was supported in part by National Institutes of Health Grants GM52801 and AI49564 (to R. A. M.). The costs of publication of this article were defrayed in part by the payment of page charges. This article must therefore be hereby marked "*advertisement*" in accordance with 18 U.S.C. Section 1734 solely to indicate this fact.

§ Present address: Max-Planck-Institut für Immunbiologie, Stübeweg 51, D-79108 Freiburg, Germany.

‖ Present address: Dept. of Natural Science and Mathematics, Concordia University, St. Paul, MN 55104.

** Supported in part by a fellowship from the Arthritis Foundation. To whom correspondence should be addressed: Center for Advanced Research in Biotechnology, W. M. Keck Laboratory for Structural Biology, University of Maryland Biotechnology Institute, 9600 Gudelsky Dr., Rockville, MD 20850. Tel.: 301-738-6119; Fax: 301-738-6255; E-mail: sundberg@umbi.umd.edu.

altered along the immunological evolutionary pathway of the catalytic antibody 48G7 in binding a *p*-nitrophenyl phosphonate hapten using surface plasmon resonance (SPR)[1] to measure equilibrium binding energies of group and individual maturation and reversion mutations (28). Cooperative contributions have been evaluated for a network of buried hydrogen bonds and salt bridges across the interface of TEM-1-β-lactamase and its protein inhibitor, BLIP (29).

The affinity maturation process, by which proteins evolve over time to bind with increased affinity and specificity, may prove especially useful for dissecting cooperative binding energetics. This approach can provide a series of variants that individually represent distinct stages of molecular evolution and together define the progression by which mutations are accumulated to construct the affinity maturation pathway. These variants act as molecular markers from which energetic and structural properties may be derived to provide insight into how mutations might act in additive or cooperative fashions with the existing molecular template from which they were derived. *In vitro* directed evolution techniques such as phage (30, 31) and yeast display (32) can be used to mimic *in vivo* affinity maturation, as they allow one to evolve proteins using the entire range of biophysical factors that govern molecular recognition. Thus, these techniques can be used as a tool to better understand how perturbations of an entire molecular interface translate to relative differences in the changes in binding energies of the resulting complexes.

Here we have attempted to expand our understanding of cooperative and additive energetics within a protein interface by elucidating equilibrium, kinetic, and thermodynamic parameters for binding of an affinity-matured protein-protein interaction. As a model system we have analyzed the affinity maturation pathway that yielded murine T cell receptor (TCR) Vβ8.2 domain variants derived from yeast display mutagenesis with up to 1500-fold increased affinity for the superantigen staphylococcal enterotoxin C3 (SEC3) (33). Iterative rounds of error-prone PCR, yeast transformation, flow cytometric selection using limiting concentrations of biotinylated ligand and sequencing resulted in an affinity maturation pathway defined by nine mutations to the wild type template: G17E, A52V, S54N, K66E, Q72H, E80V, L81S, T87S, and G96V (Fig. 1). These mutations were acquired individually or in small clusters concomitant with increased affinity for SEC3, as determined by flow cytometric titrations, in the following order: G17E ($K_D > 4$ μM); L81S ($K_D > 4$ μM); S54N, T87S, and G96V ($K_D = 217$ nM); K66E, Q72H, and E80V ($K_D = 20$ nM); and A52V ($K_D = 6$ nM). The G17E and L81S mutations have been shown previously (34) to be involved in enhanced yeast surface display and Vβ domain stability and are not likely involved in increasing the affinity for SEC3. Additionally, this is a well characterized molecular interaction for which crystallographic analysis of the wild type complex (35) as well as alanine scanning mutagenesis of both sides of the protein interface (36, 37) exist. By performing SPR analysis of group and individual maturation and reversion mutations at various temperatures, we have identified the energetically significant residues for the Vβ8.2-SEC3 affinity maturation pathway, determined the additive and cooperative effects of those mutations, and elucidated the kinetic and thermodynamic bases for molecular evolution in this protein-protein interaction system.

[1] The abbreviations used are: SPR, surface plasmon resonance; CDR, complementarity determining region; RU, response units; SEC3, staphylococcal enterotoxin C3; TCR, T cell receptor; Vβ8.2, murine TCR Vβ8.2 domain; MES, 4-morpholineethanesulfonic acid.

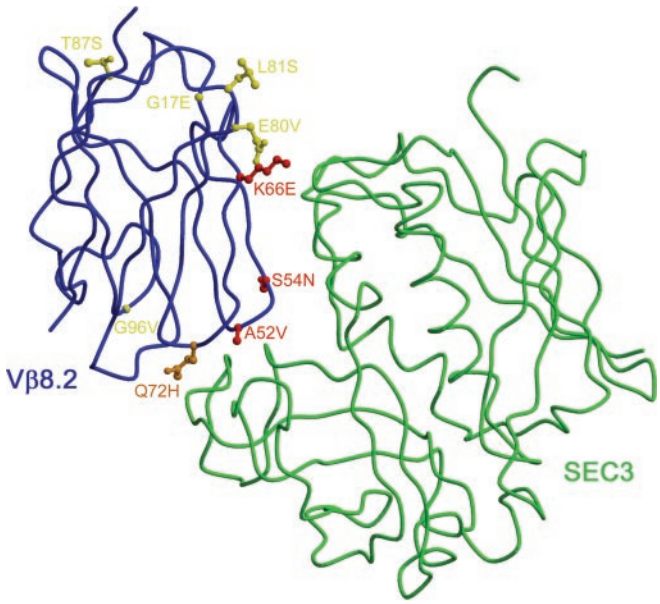

FIG. 1. **Amino acid residues altered in the affinity maturation of Vβ8.2 interaction with SEC3.** The wild type Vβ8.2-SEC3 complex as determined by x-ray crystallography (35) is shown with side chains drawn for the nine residues that differ between the low (mTCR15) and high (L2CM) affinity variants. The three Vβ8.2 variant residues (A52V (an alanine residue in mTCR15 and a valine residue in L2CM, at position 52), S54N, and K66E) that make direct intermolecular contacts with SEC3 in the wild type complex are in *red*; the Vβ8.2 variant residue (Q72H) that makes a putative contact with the mobile disulfide loop of SEC3 is in *orange*; and the remaining five Vβ8.2 variant residues (G17E, E80V, L81S, T87S, and G96V) located outside of the molecular interface are in *yellow*.

EXPERIMENTAL PROCEDURES

Protein Expression and Purification—Gene fragments encoding the low (G17E/L81S, hereafter mTCR15) and high (G17E/A52V/S54N/K66E/Q72H/E80V/L81S/T87S/G96V, hereafter L2CM) affinity murine TCR Vβ8.2 variant genes (33) were amplified using primers 5′-AAAAAAGAATTCTAGAGGCTGCAGTCACCCAAAGCCCAAG-3′ (EcoRI site underlined) and 5′-TTTTTTGGATCCTTATAGGACCGATAGTCGGGTGCCCGCACC-3′ (BamHI site underlined). Purified PCR products were digested with EcoRI and BamHI (New England Biolabs, Beverly, MA) and ligated to EcoRI-BamHI-digested pT7-7 vector (38). Maturation (A52V, S54N, K66E, Q72H, A52V/S54N, and A52V/S54N/K66E) and reversion (V52A-r, N54S-r, E66K-r, H72Q-r, V52A/N54S-r, and V52A/N54S/E66K-r) mutants were subsequently generated in mTCR15 and L2CM, respectively, by site-directed mutagenesis using a QuikChange site-directed mutagenesis kit (Stratagene, La Jolla, CA). Expression constructs were transformed into *Escherichia coli* strain BL21(DE3)pLysS (Novagen, Madison, WI), cultured in LB medium containing 100 μg/ml ampicillin and 34 μg/ml chloramphenicol, and induced at log-phase with 1 μM isopropyl-β-D-thiogalactoside for 4 h. Cells were harvested by centrifugation and lysed by sonication, and inclusion bodies were washed extensively and dissolved in 50 mM Tris-Cl, pH 8.0, 8 M urea, 10 mM dithiothreitol, 0.5 mM EDTA. Approximately 50 mg of total inclusion body material was diluted into 1 liter of refolding buffer composed of 100 mM Tris-Cl, pH 8.5, 1 M arginine, 2 mM EDTA, 6.3 mM cysteamine and 3.7 mM cystamine and incubated at 4 °C for 3 days. Concentrated refolding solution was purified by anion exchange chromatography using a Poros HQ20 column (Perspective Biosystems, Framingham, MA) equilibrated with 50 mM MES, pH 6.0, and developed with a linear NaCl gradient. Refolded Vβ8.2 variant proteins were purified further by size exclusion chromatography using an S75 column (Amersham Biosciences) in Hepes-buffered saline containing 10 mM Hepes, pH 7.5, 150 mM NaCl, 0.005% Surfactant P-20 (Biacore, Piscataway, NJ) and immediately prior to binding analysis. SEC3 was prepared according to established protocols (39).

Affinity Measurement for Equilibrium Binding—The interaction of Vβ8.2 variants with immobilized SEC3 was measured by SPR analysis using a Biacore 1000 instrument (Biacore). SEC3 protein was diluted in 10 mM sodium acetate, pH 5.0, to a concentration of 40–80 μg/ml and immobilized onto the dextran matrix of a CM5 sensor chip (Biacore)

using the amine coupling method. Typically, 300–1000 resonance units (RU) of SEC3 were immobilized. All equilibrium binding experiments were performed at 25 °C in Hepes-buffered saline buffer containing 150 mM NaCl, except for salt-dependent binding studies in which the NaCl concentration was varied. Pulses of 10 mM HCl were used to regenerate the surfaces between injections. SPR data were analyzed using BIAevaluation 3.2 software (Biacore). The association constants (K_A) were determined by steady-state affinity analysis, after correction for nonspecific binding, by measuring steady-state responses (after correction for nonspecific binding) at various concentrations, followed by nonlinear curve fitting analysis. Standard deviations for three or more independent K_A determinations were typically less than 15%.

Temperature-dependent Binding Analysis—The effect of temperature on the interaction of Vβ8.2 variants with SEC3 was measured by SPR analysis using a Biacore 3000 instrument (Biacore). To achieve optimal (80–200 RU) maximal binding of Vβ8.2 variants, 200–600 RU of SEC3 were immobilized to the CM5 chip. An unmodified dextran surface was used as a reference surface. A flow rate of 40–60 μl/min was maintained to minimize mass transfer effects. Binding experiments were performed in a temperature range of 5–35 °C. Pulses of 10 mM HCl were used to regenerate the surfaces. SPR data were analyzed using BIAevaluation 3.2 software (Biacore). For interactions with measurable on- and off-rates, k_a and k_d were fitted simultaneously using a 1:1 (Langmuir) binding model, and K_A values were determined from the ratio k_a/k_d. For those in which on- and off-rates were impossible to measure accurately, K_A values were obtained using a steady-state affinity model.

RESULTS

Relative Energetic Significance of Individual Mutations—One key requirement of an energetic analysis of molecular interactions comprising an affinity maturation pathway is the ability to measure accurately binding at both ends of the affinity range. We utilized a recombinant *E. coli* expression system to produce sufficient quantities of all Vβ8.2 variants used for the binding studies described here. SPR analysis of SEC3 interactions with both mTCR15, a Vβ8.2 variant containing two mutations (G17E/L81S) that had been shown previously to bind to SEC3 with similar affinity as wild type murine TCR Vβ8.2Cβ1 produced in myeloma cells (33, 36), and L2CM, the Vβ8.2 variant containing all nine mutations from yeast display mutagenesis, revealed that this technique was appropriate for describing the energetic parameters of the binding events at both ends of the affinity spectrum. SPR profiles for equilibrium binding of mTCR15 and L2CM to immobilized SEC3 and their corresponding steady-state affinity analyses are shown in Fig. 2. The apparent K_D values of these interactions were determined to be 7.9 μM and 5.3 nM, respectively (Table I).

The individual mutations that define the Vβ8.2 affinity maturation pathway vary in their contribution to the higher binding affinity for SEC3. The Vβ8.2-SEC3 crystal structure (35) reveals that of the nine yeast display variant sites, three Vβ8.2 residues (A52V, S54N, and K66E) make direct intermolecular contacts with SEC3, one residue (Q72H) makes a putative contact with the highly mobile disulfide loop of SEC3, and five residues (G17E, E80V, L81S, T87S, and G96V) are located outside of the molecular interface (Fig. 1). Whereas mutations to residues outside of antibody-hapten (28) or protein-protein (40) interfaces can dramatically influence the energetics or functionality of binding in some cases, SPR analysis of several combinations of mutations (Table I and Fig. 2) suggests that none of the extra-interfacial variant residues of the Vβ8.2-SEC3 complex contribute significantly to its binding energetics. Thus, the E80V, T87S, and G96V mutations may have been selected because they, like G17E and L81S, acted to increase surface level expression of the Vβ8.2-Aga2p fusion protein in the yeast display system (41). The V52A/N54S/E66K-r variant, in which these three interfacial residues have been back-mutated from the L2CM variant, and thus contains the Q72H, E80V, T87S, and G96V mutations, exhibits an increased free energy of binding to SEC3 ($\Delta\Delta G^0_{b(\text{V52A/N54S/E66K-r}-\text{mTCR15})}$) of -0.26 kcal/mol relative to the mTCR15 variant (Table I and Fig. 2). Furthermore, the Q72H variant exhibits a $\Delta\Delta G^0_{b(\text{Q72H}-\text{mTCR15})}$ of -0.48 kcal/mol. Taken together, the binding characteristics of these variants suggest that none of the extra-interfacial mutations generated by yeast display play an energetically significant role in the affinity maturation of the Vβ8.2-SEC3 complex.

In contrast, each of the three interfacial mutations and one putative interfacial mutation make important energetic contributions to the Vβ8.2-SEC3 interaction. Previous mutational analysis of residue Ala-52 had suggested this residue as a hot spot in binding (37). We observed an approximate 20-fold increase in the association constant for the A52V maturation mutation (substitution of Val for Ala at position 52 from the mTCR15 variant background), a $\Delta\Delta G^0_{b(\text{A52V}-\text{mTCR15})}$ of -1.75 kcal/mol (Table I and Fig. 2). The reversion mutation V52A-r (substitution of Ala for Val at position 52 from the L2CM background), however, exhibited a reduced $\Delta\Delta G^0_{b(\text{V52A-r}-\text{L2CM})}$ of only 0.72 kcal/mol. Residue Ser-54 behaved similarly, with an approximate 20-fold affinity increase as a maturation mutation ($\Delta\Delta G^0_{b(\text{S54N}-\text{mTCR15})} = -1.84$ kcal/mol), but a smaller decrease as a reversion mutation ($\Delta\Delta G^0_{b(\text{N54S-r}-\text{L2CM})} = 0.91$ kcal/mol). Whereas the mutations A52V and S54N are relatively conservative changes to the molecular interface, in terms of side chain size and polarity, the third interfacial mutation, K66E, is characterized by a charge reversal. This mutation provides significant energy to the interaction as evidenced by both maturation ($\Delta\Delta G^0_{b(\text{K66E}-\text{mTCR15})} = -0.88$ kcal/mol) and reversion ($\Delta\Delta G^0_{b(\text{E66K-r}-\text{L2CM})} = 1.35$ kcal/mol) mutations. The putative interfacial mutation, Q72H, exhibited a small, but significant, effect on binding as a maturation mutation ($\Delta\Delta G^0_{b(\text{Q72H}-\text{mTCR15})} = -0.49$ kcal/mol), but a negligible effect on binding as a reversion mutation ($\Delta\Delta G^0_{b(\text{Q72H-r}-\text{L2CM})} = 0.01$ kcal/mol).

Electrostatic Influence on the Binding of an Energetically Important Polar Residue—We have evaluated the equilibrium binding properties of the charge reversal mutation at position 66, as both maturation (K66E) and reversion (E66K-r) mutations, over a NaCl concentration range of 50–500 mM. The K66E variant exhibited an ~110-fold decrease in affinity for SEC3 over this ionic strength range, whereas there exists only an ~15-fold affinity reduction under similar conditions for the E66K-r variant (Fig. 3). Although the Vβ8.2-SEC3 crystal structure (35) reveals only van der Waals contacts between residue Lys-66 and SEC3 atoms, we found that electrostatic forces appear to play an important role in the selective pressure for mutation at this position in the affinity maturation pathway. The nearest charged residues in SEC3, Lys-25 and Asp-29, are ~8 and 11 Å, respectively, from the N^{ζ} atom of the Vβ8.2 K66. The electrostatic dependence of binding is more prominent in the context of the mTCR15 background (K66E variant) than in the context of the L2CM background (E66K-r variant). This may be due to the proximity of the Vβ8.2 residues at positions 80 and 66, which lie within 4 Å of one another. Although mutation of residue 80 (E80V) does not by itself contribute significantly to the energetics of binding, in combination with residue 66 it may alter the electrostatic properties of this region of Vβ8.2 enough to affect binding. The K66E maturation variant is highly electronegative in this region with two neighboring Asp residues, whereas the E66K-r reversion variant is only moderately electropositive.

Quantification of Cooperativity and Additivity—The simplest model of affinity maturation assumes that the energetic effects of all mutations are additive. Differences in binding free energy changes between maturation and reversion mutations of a common residue (Table I and Fig. 4), however, suggested a

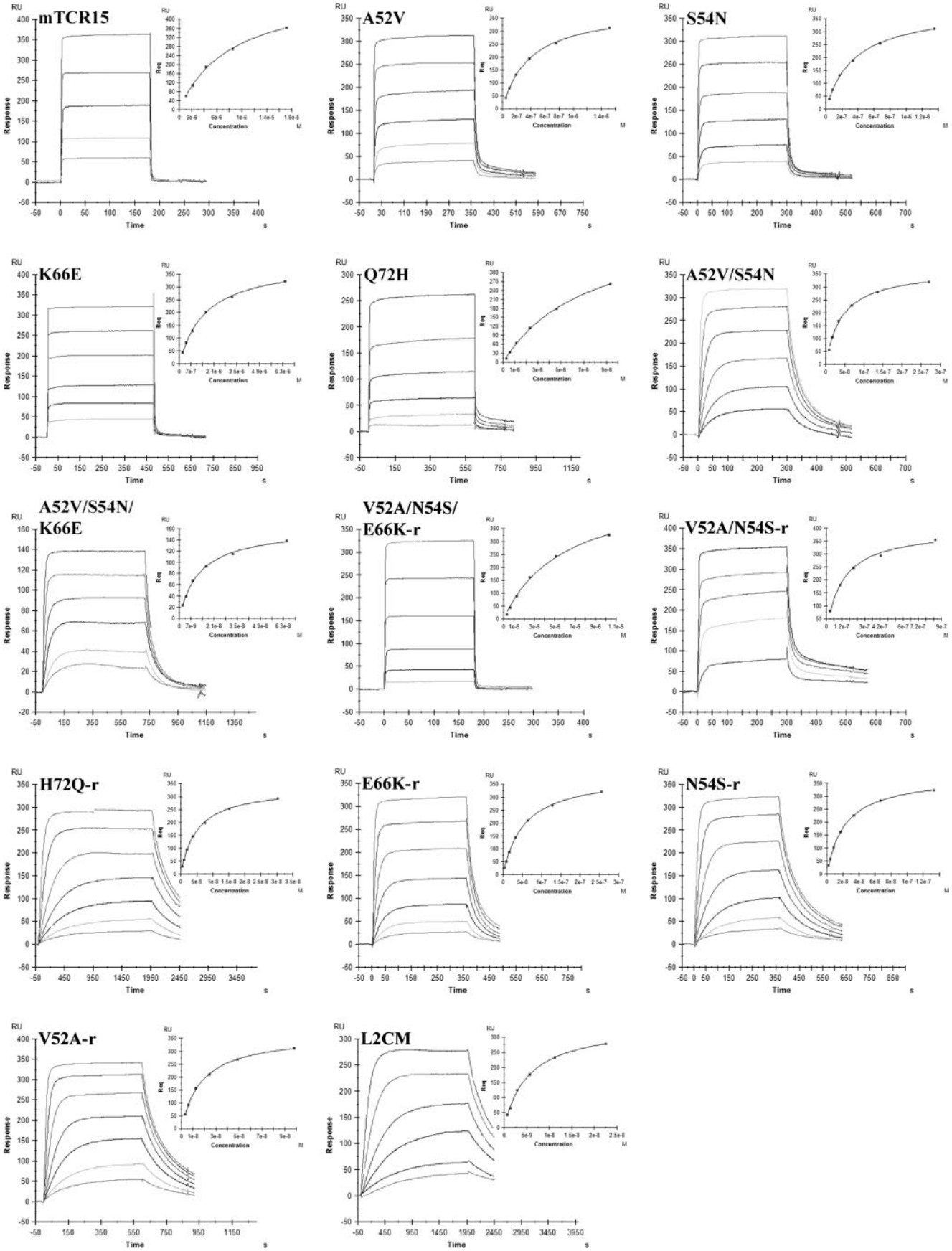

FIG. 2. **Equilibrium binding of affinity maturation variants to SEC3.** SPR sensorgrams of the interactions between mTCR15 (1070–17,100 nM), A52V (47.2–1510 nM), S54N (42.2–1350 nM), K66E (200–6430 nM), Q72H (290–9320 nM), A52V/S54N (840–27,000 nM), A52V/S54N/K66E (2.03–64.9 nM), V52A/N54S/E66K-r (320–10,300 nM), V52A/N54S-r (26.6–852 nM), H72Q-r (0.47–30.2 nM), E66K-r (3.99–255 nM), N54S-r (2.07–133 nM), V52A-r (3.06–98 nM), and L2CM (0.70–22.5 nM) with immobilized SEC3 (1000 RU) after correction for nonspecific binding. *Inset plots* show non-linear steady-state affinity analysis for each reaction.

TABLE I

Equilibrium affinity measurements for the interactions between Vβ variants and SEC3

Equilibrium affinity constants (K_A) were derived by steady-state affinity analysis of surface plasmon resonance data using three to five independent data sets. Dissociation constants (K_D) and free energies of binding (ΔG^0_b) were calculated from K_A. The changes in free energy gain and loss were determined using the free energies of mTCR15 and L2CM binding to SEC3 as references, respectively.

	K_A	K_D	ΔG^0_b	$\Delta\Delta G^0_b$ (variant-mTCR15)	$\Delta\Delta G^0_b$ (variant-L2CM)
	M^{-1}	M	*kcal/mol*	*kcal/mol*	*kcal/mol*
mTCR15	$1.31 \pm 0.07 \times 10^5$	$7.55 \pm 0.43 \times 10^{-6}$	236.98	0.00	4.30
A52V	$2.51 \pm 0.13 \times 10^6$	$3.98 \pm 0.21 \times 10^{-7}$	−8.73	−1.75	2.55
S54N	$2.92 \pm 0.09 \times 10^6$	$3.43 \pm 0.10 \times 10^{-7}$	−8.82	−1.84	2.46
K66E	$5.76 \pm 0.35 \times 10^5$	$1.74 \pm 0.11 \times 10^{-6}$	−7.86	−0.88	3.43
Q72H	$3.00 \pm 0.31 \times 10^5$	$3.36 \pm 0.37 \times 10^{-6}$	−7.47	−0.49	3.81
A52V/S54N	$2.43 \pm 0.13 \times 10^7$	$4.12 \pm 0.23 \times 10^{-8}$	−10.07	−3.09	1.21
A52V/S54N/K66E	$8.81 \pm 0.83 \times 10^7$	$1.14 \pm 0.10 \times 10^{-8}$	−10.83	−3.86	0.45
V52A/N54S/E66K-r	$2.03 \pm 0.52 \times 10^5$	$5.13 \pm 0.93 \times 10^{-6}$	−7.24	−0.26	4.04
V52A/N54S-r	$9.90 \pm 0.52 \times 10^6$	$1.01 \pm 0.05 \times 10^{-7}$	−9.54	−2.56	1.74
H72Q-r	$1.84 \pm 0.25 \times 10^8$	$5.50 \pm 0.82 \times 10^{-9}$	−11.27	−4.29	0.01
E66K-r	$1.92 \pm 0.08 \times 10^7$	$5.21 \pm 0.22 \times 10^{-8}$	−9.93	−2.96	1.35
N54S-r	$4.05 \pm 0.32 \times 10^7$	$2.48 \pm 0.19 \times 10^{-8}$	−10.37	−3.40	0.91
V52A-r	$5.57 \pm 0.11 \times 10^7$	$1.79 \pm 0.04 \times 10^{-8}$	−10.56	−3.59	0.72
L2CM	$1.87 \pm 0.07 \times 10^8$	$5.34 \pm 0.19 \times 10^{-9}$	−11.28	−4.30	0.00

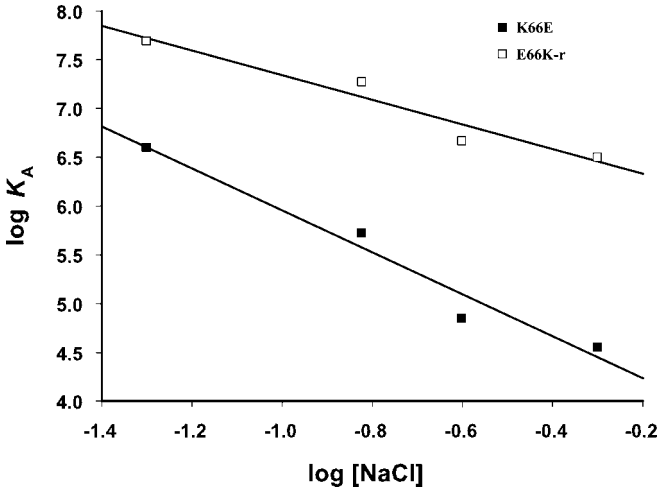

FIG. 3. **Electrostatic analysis of the binding of the K66E and E66K-r variants to SEC3.** The log values of apparent K_A values from equilibrium binding analyzed by SPR and of the NaCl concentration are plotted with the resulting slope of the linear regression a measure of the contribution of electrostatic attraction to the binding affinity, -2.15 ± 0.30 for the K66E-SEC3 interaction (*closed squares*) and -1.27 ± 0.23 for the E66K-r-SEC3 interaction (*open squares*).

significant degree of cooperativity between variant residues defined by the affinity maturation pathway. The summation of the relative differences in the changes in binding free energies of the individual maturation mutations A52V, S54N, K66E, and Q72H ($\Delta\Delta G^0_{b((A52V+S54N+K66E+Q72H)-mTCR15)} = -4.96$ kcal/mol) significantly exceeds that of L2CM ($\Delta\Delta G^0_{b(L2CM-mTCR15)} = -4.30$ kcal/mol), revealing a degree of negative cooperativity between these residues. L2CM contains three additional mutations (E80V, T87S, and G96V), by themselves energetically insignificant, beyond the four energetically important residues and the mTCR15 template for the forward mutations. These three residues could be responsible, at least in part, for the observed negative cooperativity. Likewise, these residues could also be involved in the similar magnitude cooperativity exhibited by the reversion mutation scheme ($\Delta\Delta G^0_{b((V52A-r+N54S-r+E66K-r+H72Q-r)-L2CM)} = 2.99$ kcal/mol); ($\Delta\Delta G^0_{b(mTCR15-L2CM)} = 4.30$ kcal/mol).

In order to investigate further context-dependent effects of the affinity maturation mutations, we have engineered a number of double and triple Vβ8.2 mutants and evaluated their SEC3 binding properties (Table I and Fig. 5). The double A52V/S54N maturation variant results in a $\Delta\Delta G^0_{b(A52V/S54N-mTCR15)}$ of −3.09 kcal/mol, less than the summation of the two individual maturation mutations ($\Delta\Delta G^0_{b((A52V+S54N)-mTCR15)} = -3.59$ kcal/mol), indicating negative cooperativity. In contrast, a similar double V52A/N54S-r reversion variant results in a $\Delta\Delta G^0_b$ value nearly identical to that of the summation of the individual reversion mutations ($\Delta\Delta G^0_{b(V52A/N54S-r-L2CM)} = 1.74$ kcal/mol and $\Delta\Delta G^0_{b((V52A-r+N54S-r)-L2CM)} = 1.63$ kcal/mol).

The triple A52V/S54N/K66E maturation variant exhibits a $\Delta\Delta G^0_{b(A52V/S54N/K66E-mTCR15)}$ of −3.86 kcal/mol, similar to the summation $\Delta\Delta G^0_b$ values of the double A52V/S54N and individual K66E maturation mutations ($\Delta\Delta G^0_{b((A52V/S54N+K66E)-mTCR15)} = -3.97$ kcal/mol), but significantly less than the summation of the $\Delta\Delta G^0_b$ values of all three individual maturation mutations ($\Delta\Delta G^0_{b((A52V+S54N+K66E)-mTCR15)} = -4.47$ kcal/mol). Taken together, these results suggest that the negative cooperativity inherent to the triple mutant derives predominantly from that of the A52V/S54N double mutant. The summation of the $\Delta\Delta G^0_b$ values of all three individual reversion mutations is similar to that of the double V52A/N54S-r and individual E66K-r reversion variants ($\Delta\Delta G^0_{b((V52A-r+N54S-r+E66K-r)-L2CM)} = 2.98$ kcal/mol, $\Delta\Delta G^0_{b((V52A/N54S-r + E66K-r)-L2CM)} = 3.09$ kcal/mol), whereas the triple V52A/N54S/E66K-r reversion variant confers a $\Delta\Delta G^0_{b(V52A/N54S/E66K-r-L2CM)}$ of 4.04 kcal/mol. This suggests a significant cooperative effect for the reversion variant E66K-r with residues at positions 52 and 54.

Kinetic Basis of Affinity Maturation—To establish the kinetic basis for the different affinities, we measured the on- and off-rates for variant Vβ8.2-SEC3-binding reactions. Kinetic studies were performed under lower immobilization levels and higher flow rates than equilibrium studies in order to minimize mass transport effects. We obtained temperature-dependent kinetic information for all of the Vβ8.2 variants for which we evaluated the equilibrium binding characteristics, except for the low affinity mTCR15, Q72H, and V52A/N54S/E66K-r variants. Data were fit to a 1:1 Langmuir binding model based on a single class of non-interacting binding sites using global fitting algorithms (Fig. 6). The K_A values derived from the ratio of the on- and off-rates (Table II) are in close agreement with the affinities derived from the equilibrium studies at 25 °C (Table I).

The most striking characteristic of the measured on- and off-rates is the dominant effect of the dissociation rate in the affinity maturation of the Vβ8.2-SEC3 interface. The K66E variant, the lowest affinity variant for which we were able to dependably measure kinetic parameters, exhibits a k_a value of

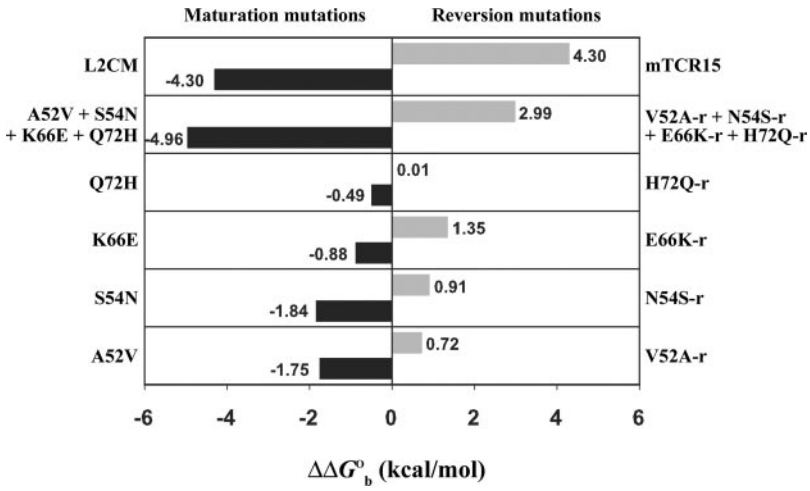

FIG. 4. **Changes in free energies of binding ($\Delta\Delta G_b^0$) associated with individual mutations.** $\Delta\Delta G_b^0$ values calculated for the individual maturation variants or summation thereof listed relative to the mTCR15-SEC3 interaction ($\Delta\Delta G^0_{b(\text{maturation})} = \Delta G^0_{b(\text{variant})} - \Delta G^0_{b(\text{mTCR15})}$; *left column*) and for the individual reversion variants or summation thereof ($\Delta\Delta G^0_{b(\text{reversion})} = \Delta G^0_{b(\text{variant})} - \Delta G^0_{b(\text{L2CM})}$; *right column*) are shown.

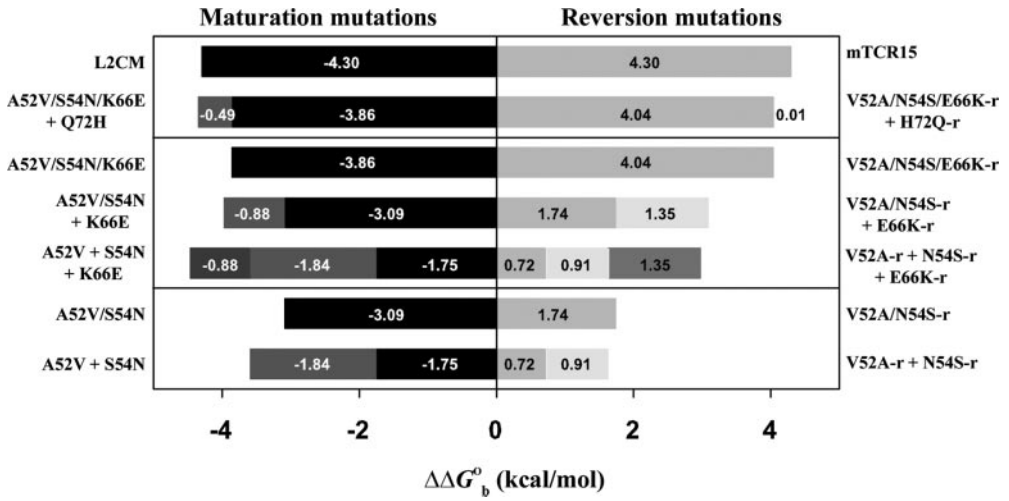

FIG. 5. **Quantification of cooperativity between maturation and reversion mutations.** Changes in the binding free energies ($\Delta\Delta G_b^0$) of selected variants incorporating single, double, or triple mutations and summations thereof are plotted for maturation (*left column*) and reversion (*right column*) mutations.

$1.77 \times 10^5\ \text{M}^{-1}\ \text{s}^{-1}$ and a k_d value of $566 \times 10^{-3}\ \text{s}^{-1}$. L2CM, the highest affinity variant and present end point of the affinity maturation pathway, is characterized by k_a and k_d values of $10.5 \times 10^5\ \text{M}^{-1}\ \text{s}^{-1}$ and $1.56 \times 10^{-3}\ \text{s}^{-1}$, respectively. This corresponds to an approximate 6-fold increase in on-rate and 360-fold decrease in off-rate. One variant, N54S-r, exhibits an on-rate that exceeds that of L2CM, whereas the L2CM off-rate is significantly reduced relative to all that of other variants.

Thermodynamic Basis of Affinity Maturation—In order to better understand the thermodynamic basis of affinity maturation, we have determined the effect of temperature on the binding of the energetically significant Vβ8.2 variants to SEC3. For each interaction, binding data were collected within the temperature range 5–35 °C. Because evaluation of the kinetics of the interactions of the lowest affinity Vβ8.2 variants mTCR15 and Q72H with SEC3 was unreliable, enthalpy values were derived from van't Hoff analysis of the temperature dependence of affinity values from equilibrium-based experiments (Table II and Fig. 7*A*). Both interactions become weaker as the temperature increases, indicative of exothermic reactions with negative enthalpies. The mTCR15 interaction with SEC3 exhibits greater temperature dependence than does that of Q72H, and as such is an enthalpically more favorable interaction. Free energy changes at 25 °C calculated from the binding affinity were used to derive entropy terms. Whereas both interactions are entropically unfavorable, the lower entropic barrier of the Q72H interaction is responsible for its increased favorable binding free energy relative to mTCR15. We were unable to obtain temperature-dependent binding data for the V52A/N54S/E66K-r interaction with SEC3.

For the remainder of the panel of Vβ8.2 variants, temperature-dependent kinetic data allowed the derivation of the activation parameters of binding. Representative Arrhenius plots for two Vβ8.2 maturation variants (L2CM and A52V/S54N/K66E) interacting with SEC3 are shown in Fig. 7*B*, from which enthalpy changes upon association ($\Delta H^{\ddagger a}$) and dissociation ($\Delta H^{\ddagger d}$) are estimated, yielding the activation enthalpy ($\Delta H^{\ddagger}$). The activation free energies of association ($\Delta G^{\ddagger a}$) and dissociation ($\Delta G^{\ddagger d}$) are calculated from the on- and off-rates at varying temperatures, together providing the activation free energy ($\Delta G^{\ddagger}$) for the reaction. Activation entropy values ($\Delta S^{\ddagger}$) are calculated from activation enthalpies and free energies ($\Delta G^{\ddagger} = \Delta H^{\ddagger} - T\Delta S^{\ddagger}$). Activation enthalpy, free energy, and entropy parameters for all Vβ8.2 variants with measurable kinetics are listed in Table II.

The present end point variants of the Vβ8.2-SEC3 affinity maturation pathway, mTCR15 and L2CM, by definition, exhibit the largest change in binding free energy. This significant improvement in affinity is due predominantly to a reduction in the entropic barriers to binding. Indeed, the L2CM-SEC3 interaction is enthalpically unfavorable relative to the majority of the variants tested. The modest gains in enthalpic terms coupled with significantly favorable entropic terms are achieved by the concerted thermodynamic changes of the energetically im-

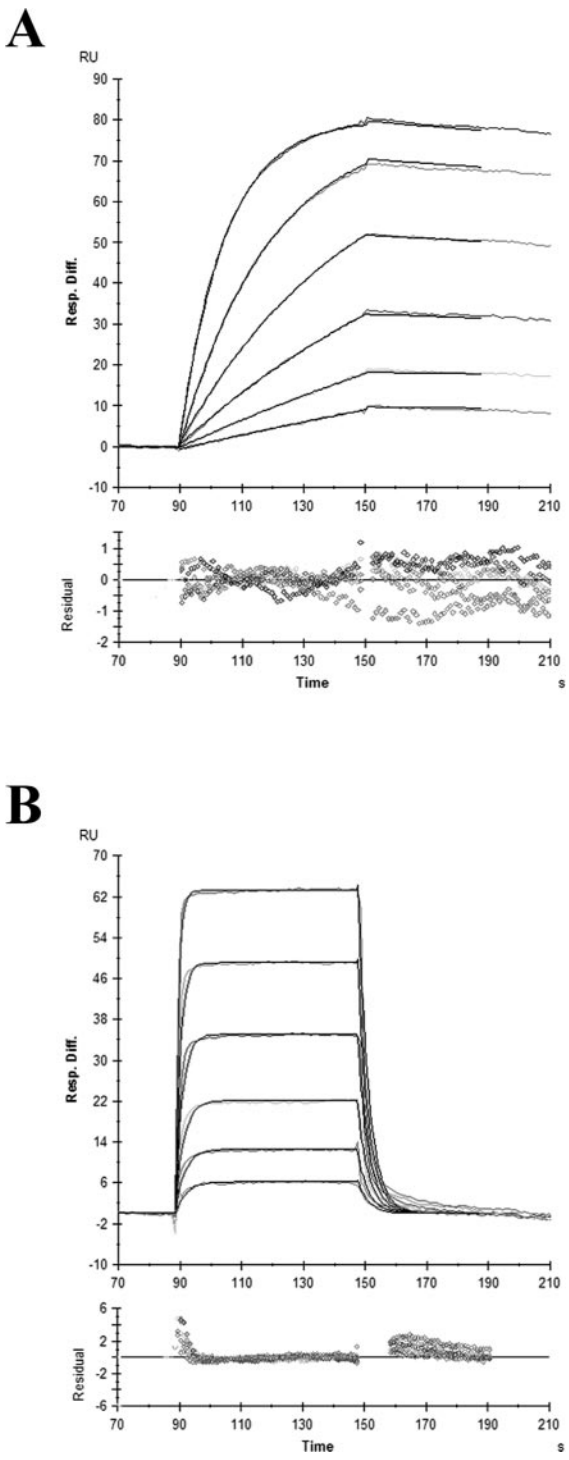

FIG. 6. **Kinetic analysis of Vβ8.2 variants binding to SEC3.** SPR sensorgrams of 2-fold dilutions of L2CM (4.5–144 nM) (*A*) and K66E (183–5860 nM) (*B*) variants binding to immobilized SEC3 (230 RU) at 5 and 15 °C, respectively. These interactions represent the highest and lowest affinity variants, respectively, for which reliable kinetic data could be obtained. Global fitting of data to a 1:1 binding model is shown in *black* and corresponding residual values are plotted *below* the individual sensorgrams.

portant variant residues. The A52V and S54N mutations are primarily responsible for any gains in enthalpy, at a small entropic cost, associated with affinity maturation. Both individual forward variants, A52V and S54N, exhibit enthalpic gains of ~2 kcal/mol, concomitant with small, unfavorable changes in entropy, relative to mTCR15. These effects are highlighted by the thermodynamic properties of the double mutations. The double A52V/S54N maturation variant exhibits the largest enthalpy change of any of the forward mutations with an entropic cost similar to the forward mutant template, mTCR15. Likewise, the double V52A/N54S-r reversion variant is the most enthalpically unfavorable and entropically favorable variant of any of the reversion mutations. Conversely, the K66E mutation results in a large enthalpic cost combined with an equally significant entropic gain, each ~5 kcal/mol, relative to mTCR15. These effects appear to be retained through the affinity maturation pathway as the addition of the K66E maturation mutation to the double A52V/S54N maturation variant, to produce the triple A52V/S54N/K66E maturation variant, results in a similar modulation of the enthalpic and entropic terms. The Q72H maturation variant behaves in a comparable, although less significant, fashion as the K66E maturation variant to decrease the entropic cost of binding with the loss of some binding enthalpy.

DISCUSSION

Molecular interfaces between interacting proteins are both structurally and energetically diverse, and as such, a functional epitope often exists whose structural components confer the great majority of binding energy in the complex and is composed of some fraction of the entire protein interface. Functional epitopes of this kind have now been mapped for numerous protein-protein interfaces (7). Within these functional epitopes exists another level of complexity, that of the structural and energetic connectivities between interfacial elements. The contributions of these discrete elements to the binding event are rarely additive but are more often cooperative in nature. Understanding this cooperativity on a quantitative level is essential to the development of predictive algorithms for protein-protein interactions. Dissection of the energetic contributions to a molecular interaction made by mutations defined by an affinity maturation pathway is one method by which to formulate a molecular basis for cooperativity between elements within a protein interface.

Although the affinity maturation pathway of the Vβ8.2-SEC3 interaction involved nine mutations that accumulated after selection by yeast display (33), we have shown here that changes in only four residues are energetically significant for binding. Together, the four individual maturation mutations (A52V, S54N, K66E, and Q72H) are nonadditive, exhibiting a $\Delta\Delta G^0_{b((A52V+S54N+K66E+Q72H)-mTCR15)}$ of −4.96 kcal/mol, compared with that of the maturation end point variant L2CM, $\Delta\Delta G^0_{b(L2CM-mTCR15)}$ of −4.30 kcal/mol, a difference of −0.66 kcal/mol. Analysis of various combinations of these mutations revealed their distinct cooperative and additive energetic effects.

The two individual maturation mutations that provide the largest individual contributions to affinity, A52V and S54N, are energetically coupled in this complex, providing the great majority of the negative cooperativity inherent to the affinity maturation pathway (compare $\Delta\Delta G^0_b$ values for the A52V + S54N and A52V/S54N variants in Fig. 5). Both of these residues are within the energetic hot spots of the Vβ8.2-SEC3 complex. In a mutational analysis of this interaction (37), an A52W variant resulted in a loss of binding free energy of more than 2 kcal/mol relative to wild type, whereas an S54A variant could not be expressed in the recombinant system being used. Furthermore, both of these residues pack against hot spot residues from the SEC3 side of the interface, including Asn-23, Tyr-90, and Gln-210 (36), according to the wild type complex structure (35). That these residues are energetically important for binding, affinity maturation, and cooperativity may be merely coincidental as non-hot spot (27) and non-contact (28) residues can have similar characteristics. Contrary to the mat-

TABLE II

Kinetic and thermodynamic parameters for interactions between Vβ8.2 variants and SEC3

Values for free energy (ΔG^0) and enthalpy (ΔH^0) were experimentally determined. ΔG^0 was determined from the relationship $\Delta G^0 = -RT \ln K_A$ and for the association and dissociation parameters from the relationships $\Delta G^{\ddagger} = -RT\,(\ln k_{on} - \ln[kT/h])$ and $\Delta G^{\ddagger d} = -RT\,(\ln k_{off} - \ln[kT/h])$, respectively, and $\Delta G^{\ddagger} = \Delta G^{\ddagger a} - \Delta G^{\ddagger d}$, where R is the gas constant; k is Boltsmann's constant, and h is Planck's constant. The overall enthalpy changes are derived from the van't Hoff analysis (slope = $\Delta H/R$) for mTCR15 and Q72H. The enthalpy changes on association and dissociation are determined from the relationships $\Delta H^{\ddagger a} = -E_a^a - RT$ and $\Delta H^{\ddagger d} = -E_a^d - RT$ where E_a values were derived from Arrhenius plots (slope = $-E_a/R$). The entropy term ($T\Delta S^0$) is calculated from the relationship $\Delta G^0 = \Delta H^0 - T\Delta S^0$, where T = 298 K.

	k_A[1]	k_d[1]	K_A	K_D	$\Delta H^{\ddagger a}$	$\Delta H^{\ddagger d}$	$\Delta H^{\ddagger}$	$\Delta G^{\ddagger}$	$T\Delta S^{\ddagger}$	$\Delta S^{\ddagger}$
	$M^{-1}\,s^{-1}$ (10^5)	s^{-1} (10^{-3})	M^{-1}	M			kcal/mol			cal/K mol
A52V	4.54	312	1.46×10^6	6.87×10^{-7}	4.10	16.40	−12.30	−8.41	−3.89	−13.00
S54N	5.60	255	2.20×10^6	4.55×10^{-7}	9.98	22.11	−12.13	−8.65	−3.48	−11.67
K66E	1.77	566	3.13×10^5	3.20×10^{-6}	5.79	11.16	−5.37	−7.50	2.13	7.14
A52V/S54N	6.62	36.2	1.83×10^7	5.47×10^{-8}	9.02	22.16	−13.14	−9.85	−3.29	−11.03
A52V/S54N/K66E	7.27	16.9	4.30×10^7	2.32×10^{-7}	9.52	15.78	−6.26	−9.02	2.76	9.26
V52A/N54S-r	7.57[2]	160[2]	4.73×10^6	2.11×10^{-7}	9.52	15.78	−6.26	−9.02	2.76	9.26
H72Q-r	9.44	5.34	1.77×10^8	5.66×10^{-7}	8.61	19.67	−11.06	−11.25	0.29	0.64
E66K-r	9.49	65.0	1.46×10^7	6.85×10^{-8}	8.87	20.72	−11.85	−9.77	−2.08	−6.98
N54S-r	11.7	30.0	3.90×10^7	2.56×10^{-8}	4.61	18.16	−13.55	−10.54	−3.01	−10.10
V52A-r	9.01	16.9	5.33×10^7	1.88×10^{-8}	8.46	19.77	−11.31	−10.54	−0.77	−2.58
L2CM	10.5	15.6	6.73×10^8	1.49×10^{-9}	6.55	17.70	−11.15	−11.39	0.24	0.80
							ΔH^0	ΔG^0	$T\Delta S^0$	ΔS^0
								kcal/mol		cal/K mol
mTCR15							−10.36	−7.11	−3.25	−10.90
Q72H							−9.48	−7.41	−2.07	−6.94
V52A/N54S/E66K-r							NA	−7.24[3]	NA	NA

[1] Kinetic parameters derived from binding analysis at 25 °C.
[2] Estimated from Arrhenius plots.
[3] Derived from equilibrium binding data, see Table I.

uration mutations, reversion mutations at positions 52 and 54 are strictly additive (compare $\Delta\Delta G_b^0$ values for the V52A-r + N54S-r and V52A/N54S-r variants in Fig. 5).

The charge reversal maturation variant K66E behaves largely in an additive fashion. As a reversion mutation, however, the E66K-r variant exhibits significant cooperativity with either or both residues at positions 52 and 54 (compare $\Delta\Delta G_b^0$ values for the V52A/N54S/E66K-r, V52A/N54S-r + E66K-r, and V52A-r + N54S-r + E66K-r variants in Fig. 5). Despite its clear energetic significance in the Vβ8.2-SEC3 affinity maturation pathway, residue Lys-66 was not identified as a hot spot for binding by alanine scanning mutagenesis (37), although the K66A variant exhibited improved binding relative to the wild type complex of −0.45 kcal/mol. Accordingly, a positive charge at this position may have a detrimental electrostatic effect. The basis for the electrostatic influence on binding associated with this charge reversal mutation (to Glu) (Fig. 3) is not clear. In the Vβ8.2-SEC3 crystal structure (35), Vβ8.2 residue Lys-66 does not form direct hydrogen bonding interactions with atoms from SEC3, but instead its intermolecular contacts are characterized by van der Waals interactions between the C^{γ} atom of Lys-66 and the phenyl ring of SEC3 residue Phe-176. These contacts could very well be conserved in the complex between SEC3 and the K66E variant. This relatively low resolution (3.5 Å) crystal structure, however, does not allow observation of water-mediated hydrogen bonds, molecular flexibility, cation-π interactions, or other factors that may have provided selective pressure for the charge reversal in the K66E affinity maturation mutation. One possibility is that the charge reversal significantly affects the long range electrostatic forces that control the on-rate, as do charge differences in other protein-protein interaction systems (42).

Mutation at position 72 appears uncoupled energetically to other residues in the interface. As a maturation mutation, the small but significant change in free energy associated with Q72H is strictly additive (compare $\Delta\Delta G_b^0$ values of the A52V/S54N/K66E and A52V/S54N/K66E + Q72H variants in Fig. 5). The reversion variant H72Q-r, however, is energetically neutral. It is noteworthy that this residue makes putative contacts with the highly mobile disulfide loop of SEC3 (35). The actual existence or transience of these contacts does not preclude this residue from providing significant or cooperative energetic contributions to the interaction, as non-contact residues can do both (28). The disulfide loop of SEC3 contains several charged residues, including three Lys residues and an Asp residue, which could affect binding differentially as the Vβ8.2 residue at position 72 varies between Gln and His.

A wide range of context-dependent effects is observed for each of these energetically significant mutation sites. Maturation and reversion variants extend from the low (mTCR15) and high (L2CM) affinity end point variants, respectively, and thus represent mutations at positions made on a background that differs by up to six residues (due to a seven-residue differential between the end point variants). Each of the four energetically important residues exhibits significantly different changes in binding free energy as maturation and reversion mutations (Fig. 4). This phenomenon was also observed for the energetics of binding in the affinity maturation of the antibody 48G7 (28) and is indicative of cooperativity between the mutated residue and its interfacial partners. The cooperative and additive characteristics of the mutations are themselves context-dependent. For instance, A52V and S54N are cooperative as maturation mutations but additive as reversion mutations, whereas K66E is additive in maturation but cooperative as a reversion mutation (Fig. 5).

The kinetic and thermodynamic bases of the Vβ8.2-SEC3 directed evolution pathway have been elucidated. Kinetically, affinity maturation is dominated by reduction of the off-rate, which is ~60 times more effective than the on-rate in increasing apparent K_A. This may be a result of an increase in the buried hydrophobic surface area resulting from the A52V and S54N mutations. Off-rate reduction represents only one route to improved affinity, as a TEM-1-β-lactamase-BLIP complex has been designed with 250-fold increases in on-rate and affinity and a constant off-rate (43). TCR molecules that have been affinity-matured by yeast display for binding to peptide-major histocompatibility complexes also exhibit greater influences from on-rates (12–110-fold faster) than from off-rates (up to

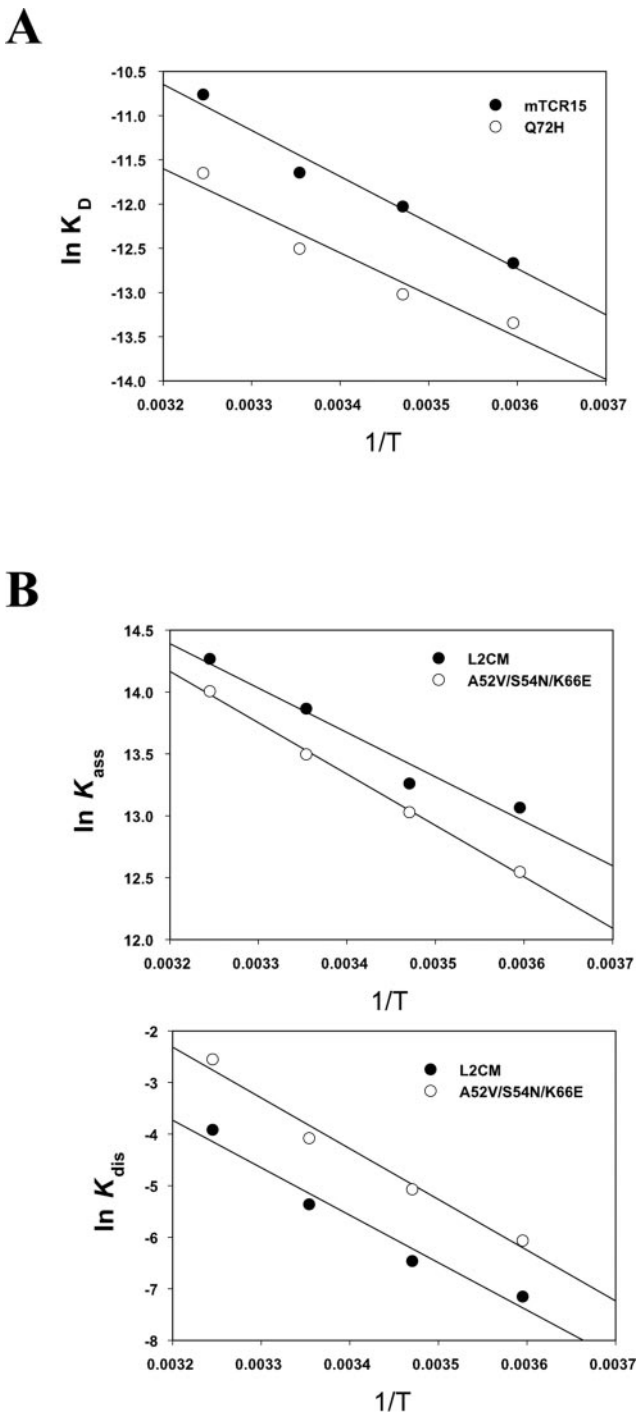

FIG. 7. **Thermodynamic analysis of Vβ8.2 variants binding to SEC3.** *A*, van't Hoff analysis of affinity as a function of temperature in which ln K_D values from equilibrium-based affinity measurements are plotted against inverse temperature for mTCR15 (*closed circles*) and Q72H (*open circles*) variants. Enthalpy changes (ΔH) are derived from the resulting linear regression. As ΔH can change with temperature, van't Hoff plots are not strictly linear, and the ΔH values obtained apply with highest precision at the midpoint of the range of temperatures used for the fit. *B*, Arrhenius plots of ln k_a (*upper panel*) and ln k_d (*lower panel*) versus inverse temperature for the L2CM (*closed circles*) and A52V/S54N/K66E (*open circles*) variants binding to SEC3. The variation of the association and dissociation rates with temperature determines the slope of the curve from which the enthalpies of association ($\Delta H^{\ddagger a}$) and dissociation ($\Delta H^{\ddagger d}$) can be determined, respectively ($\Delta H^{\ddagger a} = -E_a^a - RT$; $\Delta H^{\ddagger d} = -E_a^d - RT$; ($\Delta H^{\ddagger} = \Delta H^{\ddagger a} - \Delta H^{\ddagger d}$).

30-fold slower) (44). Thermodynamically, fully four-fifths of the decrease in binding free energy is a result of the reduction of entropic barriers to complex formation. This represents a balance, however, between the enthalpic advantage/entropic disadvantage of the A52V and S54N mutations with the entropic advantage/enthalpic disadvantage of the K66E mutation.

As the Vβ8.2 residues at positions 52 and 54, together with a glycine residue at position 53, form the apical region of the CDR2 loop of this Ig domain, it is enticing to ascribe their negative cooperativity to a concerted structural rearrangement of this loop. Both structural (45–48) and energetic (49–51) studies have indicated that conformational flexibility of TCR molecules is a common feature in their recognition of peptide-major histocompatibility complexes. This TCR plasticity is largely attributable to ligand-induced movement of the CDR3 loops, which are not involved in the Vβ8.2-SEC3 interaction (35). Although the affinity maturation of Vβ8.2 is dominated by reduction of the off-rate, there still exists a significant (at least 10-fold) increase in on-rate between the mTCR15 and L2CM variants. This implies that portions of the TCR Vβ domain that contain the energetically significant mutations, namely the CDR2 loop (residues 52 and 54), framework region 3 (residue 66), and hypervariable region 4 (residue 72), may be flexible and that some or all of these mutations confer increased affinity by altering this mobility.

It is somewhat surprising that the cooperativity exhibited by the affinity maturation pathway of the Vβ8.2-SEC3 interaction is negative. The immunological evolutionary pathway of the 48G7 antibody from its germ line to mature forms, concomitant with increased affinity for its hapten by ~3000-fold, invokes positive cooperativity through numerous residues (28). Together, the summation of the $\Delta\Delta G_b^0$ values of the individual maturation mutations is 19% lower than that of the mature antibody, into which all of these mutations are incorporated concurrently ($\Delta\Delta G^0_{b(\Sigma\text{somatic mutations})} = -3.8$ kcal/mol; $\Delta\Delta G^0_{b(\text{mature 48G7})} = -4.7$ kcal/mol). The affinity maturation pathways of two other antibody-hapten systems, with significantly smaller affinity differences between the germ line and mature complexes, have been energetically dissected and their maturation mutations found to be additive (52, 53). It was presumed that positive cooperativity was a useful, if not required, mechanism to bridge such large affinity gaps. The cooperative energetics of the Vβ8.2-SEC3 affinity maturation pathway, however, provides a counter-example. Whereas the affinity difference between the end point variants mTCR15 and L2CM, ~1500-fold, is similar to that of the 48G7 germ line and mature antibodies, the summation of $\Delta\Delta G_b^0$ values of the individual maturation mutations instead exceeds that of L2CM, into which all of these individual mutations are incorporated concurrently, by 15% ($\Delta\Delta G^0_{b((\text{A52V+S54N+K66E+Q72H})-\text{mTCR15})} = -5.02$ kcal/mol; $\Delta\Delta G^0_{b(\text{L2CM}-\text{mTCR15})} = -4.33$ kcal/mol). This may be indicative of the differences between the affinity maturation mechanisms for antibody-hapten complexes, in which there exist discrete hot spots for mutation (54) and which can utilize up to two Ig domains and 6 CDR loops, compared with the Vβ8.2-SEC3 interaction which operates, to a large extent, on more conserved Ig residues and one CDR loop.

Alternatively, these findings may represent just two disparate examples from the wide spectrum of mechanisms that can yield affinity-matured interactions. Additional antibody and Vβ domain engineering studies will be needed to address this issue. It may also suggest a marginal utility of further modification of the binding interface. As the final step in the molecular evolution of this interaction, the A52V mutation is beneficial to the minimization of the binding free energy but not to the extent to which it can improve binding when added to the low affinity template mTCR15.

The complexities of cooperative binding energetics represent a formidable barrier to the quantitative understanding of pro-

tein-protein interactions. Accordingly, the dissection of such cooperative effects on protein binding is crucial to the development of algorithms that reliably correlate structural and energetic parameters of molecular interaction.

Acknowledgment—We thank Dr. Peter S. Andersen for critical reading of the manuscript.

REFERENCES

1. Wodak, S. J., and Janin, J. (2002) *Adv. Protein Chem.* **61,** 9–73
2. Sundberg, E. J., Andersen, P. S., Schlievert, P. M., Karjalainen, K., and Mariuzza, R. A. (2003) *Structure* **11,** 1151–1161
3. Li, Y., Li, H., Yang, F., Smith-Gill, S. J., and Mariuzza, R. A. (2003) *Nat. Struct. Biol.* **10,** 482–488
4. Sundberg, E. J., and Mariuzza, R. A. (2000) *Struct. Fold. Des.* **8,** R137–R142
5. Bogan, A. A., and Thorn, K. S. (1998) *J. Mol. Biol.* **280,** 1–9
6. Conte, L. L., Chothia, C., and Janin, J. (1999) *J. Mol. Biol.* **285,** 2177–2198
7. DeLano, W. L. (2002) *Curr. Opin. Struct. Biol.* **12,** 14–20
8. Ma, B., Wolfson, H. J., and Nussinov, R. (2001) *Curr. Opin. Struct. Biol.* **11,** 364–369
9. Sheinerman, F. B., Norel, R., and Honig, B. (2000) *Curr. Opin. Struct. Biol.* **10,** 153–159
10. Sundberg, E. J., Urrutia, M., Braden, B. C., Isern, J., Tsuchiya, D., Fields, B. A., Malchiodi, E. L., Tormo, J., Schwarz, F. P., and Mariuzza, R. A. (2000) *Biochemistry* **39,** 15375–15387
11. Brooijmans, N., Sharp, K. A., and Kuntz, I. D. (2002) *Proteins* **48,** 645–653
12. Hilser, V. J., Gomez, J., and Freire, E. (1996) *Proteins* **26,** 123–133
13. Kuntz, I. D., Chen, K., Sharp, K. A., and Kollman, P. A. (1999) *Proc. Natl. Acad. Sci. U. S. A.* **96,** 9997–10002
14. Lavigne, P., Bagu, J. R., Boyko, R., Willard, L., Holmes, C. F., and Sykes, B. D. (2000) *Protein Sci.* **9,** 252–264
15. Luque, I., and Freire, E. (2002) *Proteins* **49,** 181–190
16. Wells, J. A. (1990) *Biochemistry* **29,** 8509–8517
17. Cunningham, B. C., and Wells, J. A. (1991) *Proc. Natl. Acad. Sci. U. S. A.* **88,** 3407–3411
18. Jin, L., and Wells, J. A. (1994) *Protein Sci.* **3,** 2351–2357
19. Muller, Y. A., Chen, Y., Christinger, H. W., Li, B., Cunningham, B. C., Lowman, H. B., and de Vos, A. M. (1998) *Structure* **6,** 1153–1167
20. Kelley, R. F., and O'Connell, M. P. (1993) *Biochemistry* **32,** 6828–6835
21. Dall'Acqua, W., Goldman, E. R., Eisenstein, E., and Mariuzza, R. A. (1996) *Biochemistry* **35,** 9667–9676
22. Chen, C. Z., and Shapiro, R. (1999) *Biochemistry* **38,** 9273–9285
23. LiCata, V. J., and Ackers, G. K. (1995) *Biochemistry* **34,** 3133–3139
24. Shapiro, R., Ruiz-Gutierrez, M., and Chen, C. Z. (2000) *J. Mol. Biol.* **302,** 497–519
25. Schreiber, G., and Fersht, A. R. (1995) *J. Mol. Biol.* **248,** 478–486
26. Goldman, E. R., Dall'Acqua, W., Braden, B. C., and Mariuzza, R. A. (1997) *Biochemistry* **36,** 49–56
27. Teufel, D. P., Kao, R. Y., Acharya, K. R., and Shapiro, R. (2003) *Biochemistry* **42,** 1451–1459
28. Yang, P. L., and Schultz, P. G. (1999) *J. Mol. Biol.* **294,** 1191–1201
29. Albeck, S., Unger, R., and Schreiber, G. (2000) *J. Mol. Biol.* **298,** 503–520
30. Lowman, H. B. (1997) *Annu. Rev. Biophys. Biomol. Struct.* **26,** 401–424
31. Winter, G., Griffiths, A. D., Hawkins, R. E., and Hoogenboom, H. R. (1994) *Annu. Rev. Immunol.* **12,** 433–455
32. Boder, E. T., and Wittrup, K. D. (1997) *Nat. Biotechnol.* **15,** 553–557
33. Kieke, M. C., Sundberg, E., Shusta, E. V., Mariuzza, R. A., Wittrup, K. D., and Kranz, D. M. (2001) *J. Mol. Biol.* **307,** 1305–1315
34. Shusta, E. V., Holler, P. D., Kieke, M. C., Kranz, D. M., and Wittrup, K. D. (2000) *Nat. Biotechnol.* **18,** 754–759
35. Fields, B. A., Malchiodi, E. L., Li, H., Ysern, X., Stauffacher, C. V., Schlievert, P. M., Karjalainen, K., and Mariuzza, R. A. (1996) *Nature* **384,** 188–192
36. Leder, L., Llera, A., Lavoie, P. M., Lebedeva, M. I., Li, H., Sekaly, R. P., Bohach, G. A., Gahr, P. J., Schlievert, P. M., Karjalainen, K., and Mariuzza, R. A. (1998) *J. Exp. Med.* **187,** 823–833
37. Churchill, H. R., Andersen, P. S., Parke, E. A., Mariuzza, R. A., and Kranz, D. M. (2000) *J. Exp. Med.* **191,** 835–846
38. Tabor, S., and Richardson, C. C. (1985) *Proc. Natl. Acad. Sci. U. S. A.* **82,** 1074–1078
39. Andersen, P. S., Lavoie, P. M., Sekaly, R. P., Churchill, H., Kranz, D. M., Schlievert, P. M., Karjalainen, K., and Mariuzza, R. A. (1999) *Immunity* **10,** 473–483
40. Carson, R. T., Vignali, K. M., Woodland, D. L., and Vignali, D. A. (1997) *Immunity* **7,** 387–399
41. Shusta, E. V., Kieke, M. C., Parke, E., Kranz, D. M., and Wittrup, K. D. (1999) *J. Mol. Biol.* **292,** 949–956
42. Schreiber, G. (2002) *Curr. Opin. Struct. Biol.* **12,** 41–47
43. Selzer, T., Albeck, S., and Schreiber, G. (2000) *Nat. Struct. Biol.* **7,** 537–541
44. Holler, P. D., and Kranz, D. M. (2003) *Immunity* **18,** 255–264
45. Garcia, K. C., Degano, M., Pease, L. R., Huang, M., Peterson, P. A., Teyton, L., and Wilson, I. A. (1998) *Science* **279,** 1166–1172
46. Ding, Y. H., Baker, B. M., Garboczi, D. N., Biddison, W. E., and Wiley, D. C. (1999) *Immunity* **11,** 45–56
47. Reiser, J. B., Darnault, C., Gregoire, C., Mosser, T., Mazza, G., Kearney, A., van der Merwe, P. A., Fontecilla-Camps, J. C., Housset, D., and Malissen, B. (2003) *Nat. Immun.* **4,** 241–247
48. Reiser, J. B., Gregoire, C., Darnault, C., Mosser, T., Guimezanes, A., Schmitt-Verhulst, A. M., Fontecilla-Camps, J. C., Mazza, G., Malissen, B., and Housset, D. (2002) *Immunity* **16,** 345–354
49. Boniface, J. J., Reich, Z., Lyons, D. S., and Davis, M. M. (1999) *Proc. Natl. Acad. Sci. U. S. A.* **96,** 11446–11451
50. Anikeeva, N., Lebedeva, T., Krogsgaard, M., Tetin, S. Y., Martinez-Hackert, E., Kalams, S. A., Davis, M. M., and Sykulev, Y. (2003) *Biochemistry* **42,** 4709–4716
51. Willcox, B. E., Gao, G. F., Wyer, J. R., Ladbury, J. E., Bell, J. I., Jakobsen, B. K., and van der Merwe, P. A. (1999) *Immunity* **10,** 357–365
52. Romesberg, F. E., Spiller, B., Schultz, P. G., and Stevens, R. C. (1998) *Science* **279,** 1929–1933
53. Ulrich, H. D., Mundorff, E., Santarsiero, B. D., Driggers, E. M., Stevens, R. C., and Schultz, P. G. (1997) *Nature* **389,** 271–275
54. Green, N. S., Lin, M. M., and Scharff, M. D. (1998) *BioEssays* **20,** 227–234